International Journal of Nature and Life Sciences

IJNLS

https://dergipark.org.tr/tr/pub/ijnls

e-ISSN: 2602-2397 https://doi.org/10.47947/ijnls.1591265

Research Article

Spectroscopic, Crystallographic and Thermal Comparison of Two Asymmetric Tridentate Schiff Base Molecules

Alper Yardan [1*], Cenk Paşa [2]

[1] Property Protection and Security Department, Occupational Health and Safety Programme, Dursunbey Vocational School, Balıkesir University, Dursunbey, Balıkesir, Türkiye.; https://orcid.org/0000-0001-6916-831X

[2] Department of Plant and Animal Production, Medicinal and Aromatical Plant Programme, Altınoluk Vocational School, Balıkesir University, Edremit, Balıkesir, Türkiye.; https://orcid.org/0000-0002-6125-9767

*** Corresponding author:** alperyardan@gmail.com

Received: November 26, 2024

Accepted: December 14, 2024

Published: December 30, 2024

Citation: Yardan, A., & Paşa, C. (2024). Spectroscopic, crystallographic and thermal comparison of two asymmetric tridentate schiff base molecules. International Journal of Nature and Life Sciences, 8 (2), 228-240.

Abstract: Two similar asymmetric ONO type tridentate Schiff Base ligand molecules and their spectroscopic, crystallographic and thermal properties are comparised. Both of molecules obtained in the study were characterized by ^{1}H-NMR, ^{13}C-NMR, thermal analysis, IR spectroscopy and UV-Vis spectroscopy. However molecules were able to be obtained as single crystals and their structures were determined by single crystal X-ray technique. The space group of the geometric shape of the 2'-(2-hydroxy-anilidene)-4-hydroxy-pentane (L_1) ligand is $P2_12_12_1$. There are 4 molecules in the unit cell of the crystal system of the L_1 ligand. The space group of the geometric shape of the 4'(2-hydroxy-5-chlorine-anilidene)-2-hydroxy-pentane (L_2) ligand is $P2_1/c$. There are four molecules in the unit cell of the crystal system of the ligand. Although they are ligands with similar structure, L_1 ligand has an orthorhombic unit cells and L_2 ligand has a monoclinic unit cells. Thermal analysis of the ligands showed a state change point. L_1 and L_2 ligands degraded in a single step. The ^{1}H-NMR spectra of the L_1 and L_2 ligands, which have similar structures, are similar in outline. However, it is interesting to observe that the peaks of these carbons are observed in a higher area since the chlorine atom attached to the aromatic ring in the L_2 ligand increases the screening effect.. The spectroscopic results also show a general similarity, but the effect of the chlorine atom stands out.

Keywords: ONO type ligand, Thermal analysis, Schiff base, Single crystal X-ray technique, Spectroscopy.

1. Introduction

Schiff bases and their complexes are of interest to biologists, physicists and other scientists as well as chemists. There are many publications in the literature examining the behavior of Schiff base complexes such as biological activity and magnetic properties (Dalei et al., 2024; Wang et al., 2024; Yardan et al., 2014). In living organisms, many biochemical reaction steps are known to proceed through Schiff bases (Yardan et al., 2015). This once again proves the importance of Schiff bases.

Schiff bases are widely used because they are stable and easy to synthesize. Schiff bases or Azomethines are used in many biological fields, especially in antioxidant, antifungal, antitumor, antibacterial, antipyretic and anti-inflammatory applications (Li et al., 2022; Yardan et al., 2015; Tian et al., 2016). The

importance of Schiff base structures in medicine and pharmacology is more interesting because of their anticancer activity properties. At the same time, their metal complexes have been widely studied because of their anticancer and herbicide applications (Sharma et al., 2024; Wang et al., 2014). Especially antifungal and herbicide applications in agriculture is getting higher attention in recent years (Azadi et al., 2024; Puthilibai et al., 2023; Zhang et al., 2024). In addition to TG and DTA are important in the study of thermal properties of compounds techniques (Choudhary, 2023; Moreira et al., 2025; Nassar et al., 2024). The study of their thermal behavior has recently attracted intense interest (Abdel-Rahman et al., 2017; Somashekar et al., 2022).

In this study, two asymmetric ONO type tridentate Schiff Base ligand comparised by UV-Vis spectroscopy, IR spectroscopy, thermal analysis, ^{1}H-NMR and ^{13}C-NMR and single crystal XRD technique. Here, the thermal and spectrochemical properties of the ligands have been investigated to contribute to the literature.

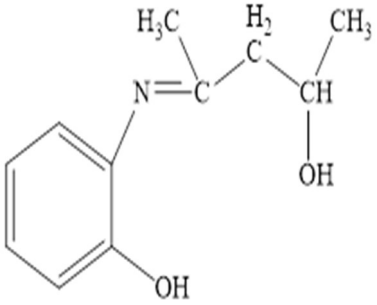

Figure 1. L_1 ligand

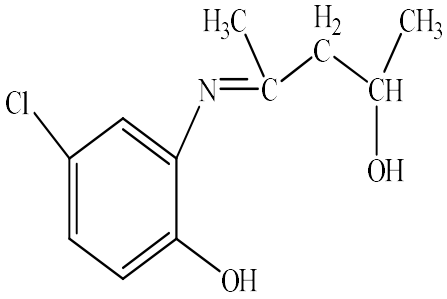

Figure 2. L_2 ligand

2. Materials and Methods

i) IR studies were performed using a Perkin Elmer 1600 Series FT-IR spectrometer

The spectra of the compounds were recorded in the range of 4000-400 cm^{-1} by KBr disk technique.

ii) ^{1}H-NMR and ^{13}C-NMR analyses were performed with a Bruker Ultrashield Superconducting 400 MHz liquid NMR spectrometer.

iii) Single crystal XRD analyses were performed Bruker SMART CCD field-detector diffractometer using Mo-Kα beam

iv) The electronic spectra of the complexes were recorded in the range of 200-900 nm on a Perkin Elmer Lambda 25 UV-Vis spectrophotometer using DMSO as solvent. For the calculation of the molar absorption coefficient, calibration curves were drawn by preparing working solutions in the concentration range of 10^{-3} M stock solutions (1.10^{-6}-1.10^{-4}M). The slopes of the calibration curves were used to calculate the molar absorption coefficients.

v) Perkin-Elmer Diamond brand Thermal Analyzer was used for thermogravimetric analysis. TG, DTG and DTA curves were recorded simultaneously.

3. Results

3.1. IR spectroscopy

It is seen that the IR spectra of L_1 and L_2, which are ONO type ligands with similar structure, are similar. The C=N peak of the L_1 ligand is at 1606 cm^{-1} while the C=N peak of the L_2 ligand is at 1607 cm^{-1}.

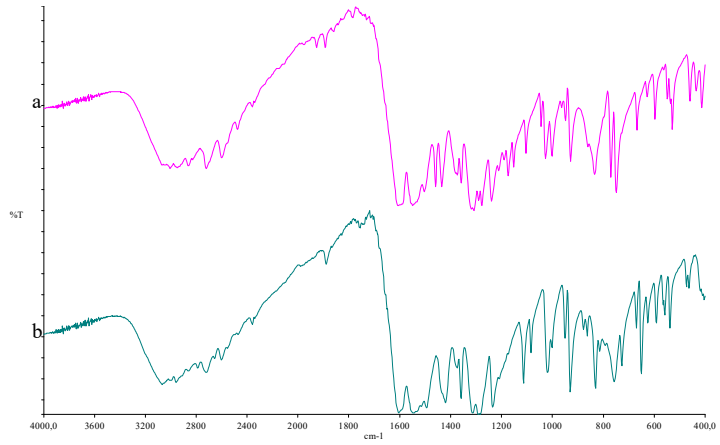

Figure 3. Spectrums of the ligands (a) L_1, (b) L_2

3.2. UV-Vis spectroscopy

10^{-3} M solutions of the ligands in DMSO were prepared and 1.10^{-6}, 4.10^{-6}, 8.10^{-6}, 1.10^{-5}, 4.10^{-5}, 8.10^{-5} and 1.10^{-4} M dilute solutions were prepared from the stock solution. The UV-Vis spectra of the compounds in the wavelength range of 200-900 nm were first recorded and the wavelengths at which they gave maximum absorptivity were determined for each molecule. Absorbtivity values were recorded at the wavelengths determined with the prepared working solutions and absorptivity-concentration curves were drawn (Figures 4-5). Using these calibration curves, the molar absorption coefficients were found for each compound at the wavelengths determined. Table 1 shows the UV-Vis results of the ligands.

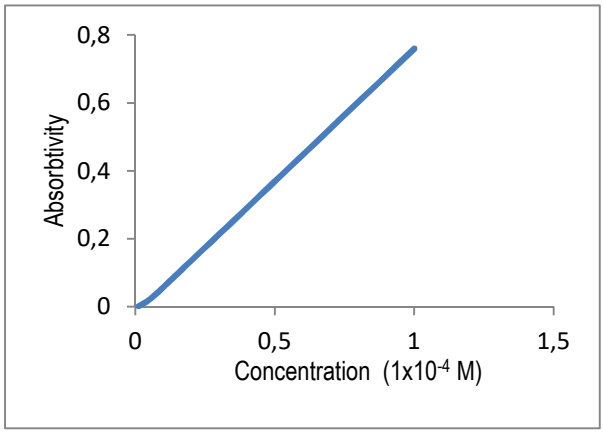

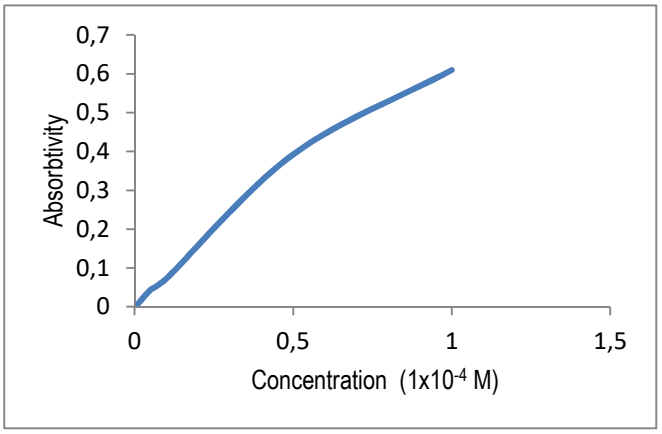

Figure 4. Absorbtivity-concentration curve of L_1 ligand (λ=297 nm).

Figure 5. Absorbtivity-concentration curve of L_2 ligand (λ=240 nm).

Table 1. UV-Vis. Values of the ligands.

Ligands	**λ_{max} nm , (ε) M^{-1} . cm^{-1}**
L_1	234 (3650) ; 297 (7720) ; 364 (4400)
L_2	240 (6200) ; 283 (3920) ; 368 (4900)

3.3. NMR studies

3.3.1. ^{1}H-NMR studies

Unlike most other Schiff Base ligands, the L_1 ligand has no hydrogen attached to the imine group. Therefore, a peak between 8 and 9 ppm was not observed. The phenolic OH peak of the ligand appeared at 12.2 ppm and the aliphatic OH peak appeared at 9.9 ppm (Figure 6).

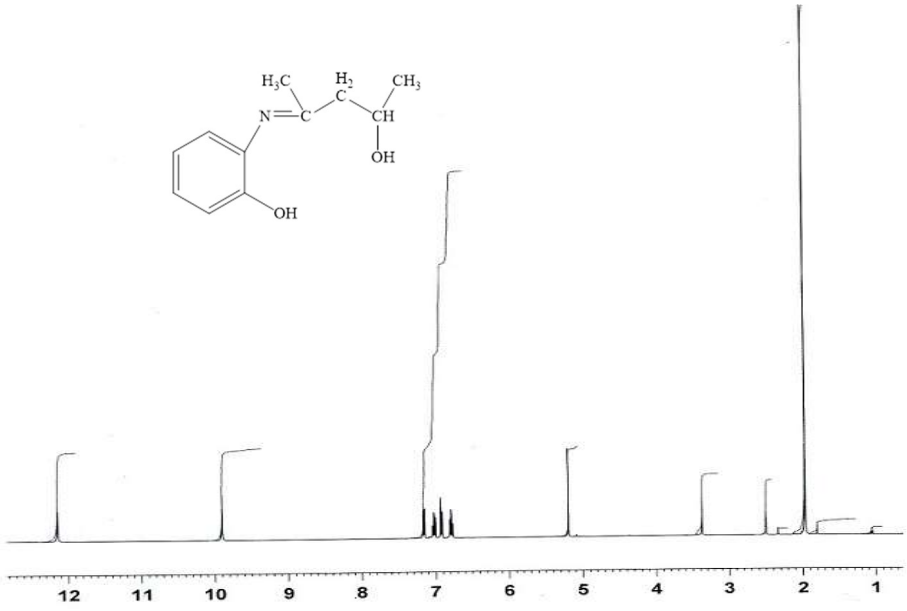

Figure 6. ^{1}H-NMR spectrum of L_1 ligand in DMSO at 300 K and 400 MHz.

There is also no hydrogen in the imine group in the L_2 ligand. Therefore, no peak was observed between 8 and 9 ppm. In this ligand, OH peak is observed at two different positions. Among these, phenolic OH resonates at 12.16 ppm and OH due to aliphatic group resonates at 10.25 ppm (Figure 7).

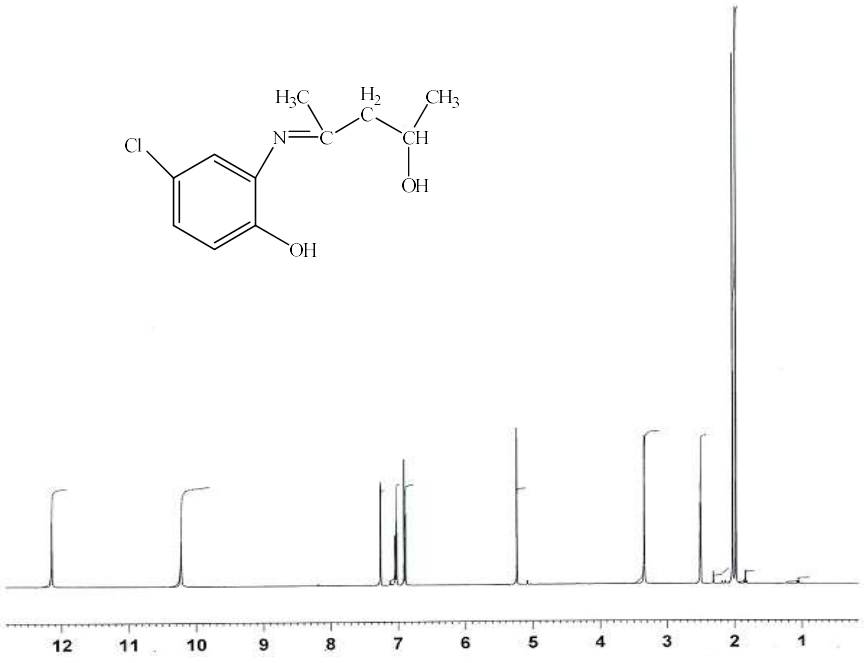

Figure 7. ^{1}H-NMR spectrum of L_1 ligand in DMSO at 300 K and 400 MHz.

3.3.2. ^{13}C-NMR studies

When the 13C-NMR spectrum of the L_1 ligand is examined, it is seen that the peak belonging to the imine carbon appears at a lower area (194 ppm) than the ligands previously examined (Figure 8). The main reason for this is the methyl group attached to the imine group.

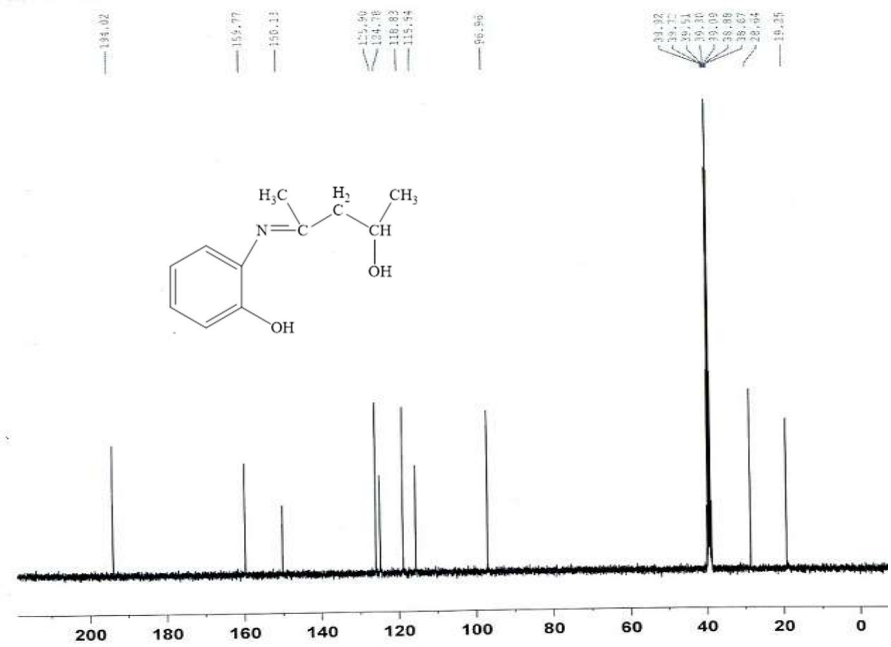

Figure 8. ^{13}C-NMR spectrum of L_1 ligand in DMSO at 300 K and 100 MHz.

The peak of the imine carbon in the L_2 ligand is observed at 194 ppm (Figure 9). The low area of this value is due to the methyl group attached to the imine carbon.

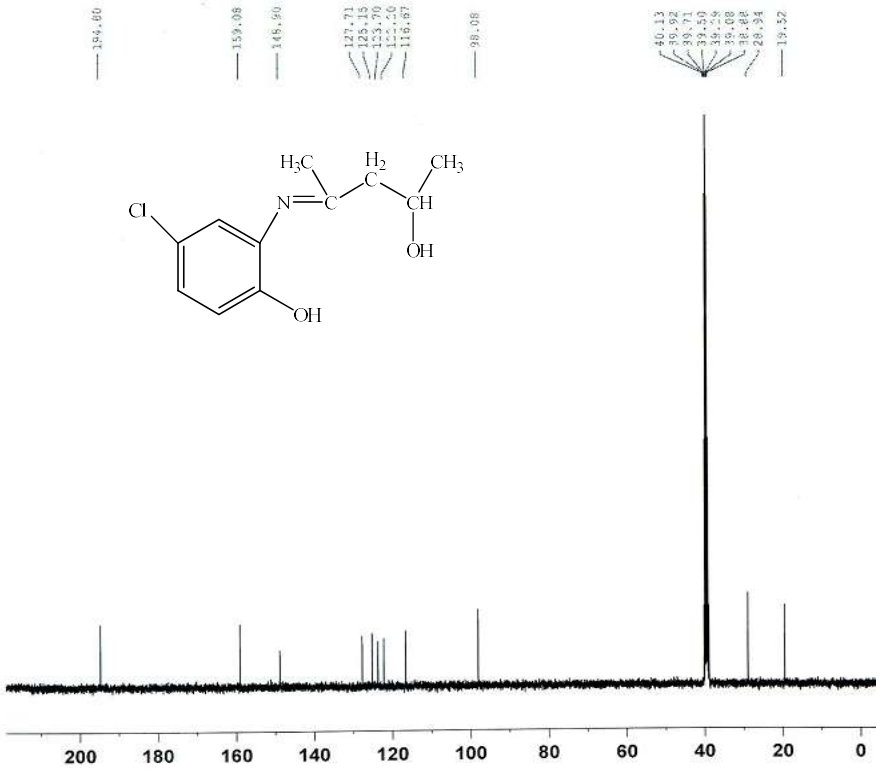

Figure 9. ^{13}C-NMR spectrum of L_2 ligand in DMSO at 300 K and 100 MHz.

3.4. TG and DTA curves of ligands

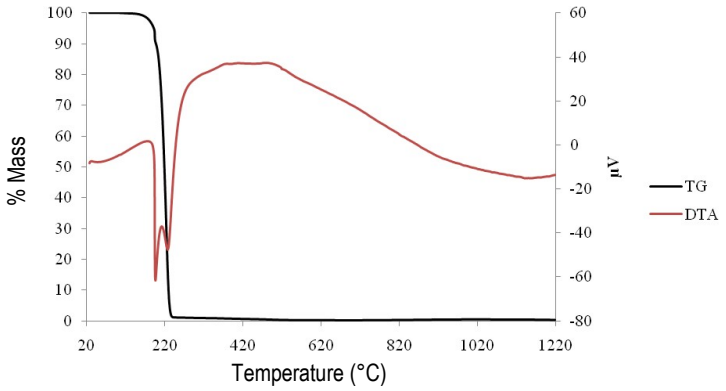

Figure 10. TG and DTA curves of L_1.

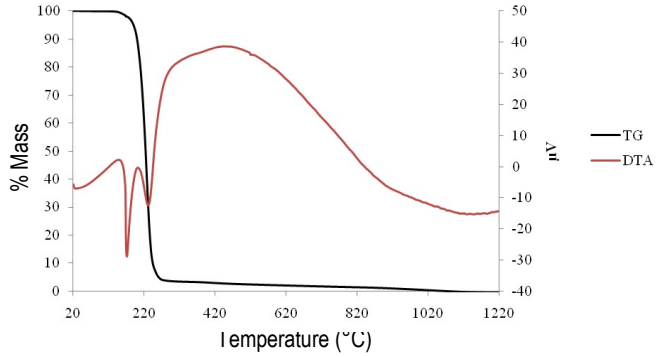

Figure 11. TG and DTA curves of L_2.

Two consecutive endothermic peaks are observed in the DTA curve of L_1 ligand. The first of these peaks appeared at 196 °C and the second at 231 °C (Figure10). It can also be seen from the TG curve that the substance degrades in this temperature range. In the DTA curve of L_2 ligand, two different peaks are observed at 172 °C and 235 °C. It can be stated that the ligand decomposes in this temperature range (Figure 11). This is also consistent with the mass loss observed in the TG curve.

3.5. Single crystal X-Ray studies

3.5.1. Single crystal X-Ray studies of L_1 ligand

The single crystal X-ray results of the L_1 are given in Table 2 and the selected bond lengths and bond angles of the ligand are given in Table 3.

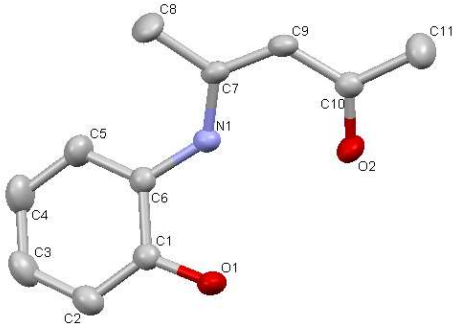

Figure 12. Crystal structure of the L_1.

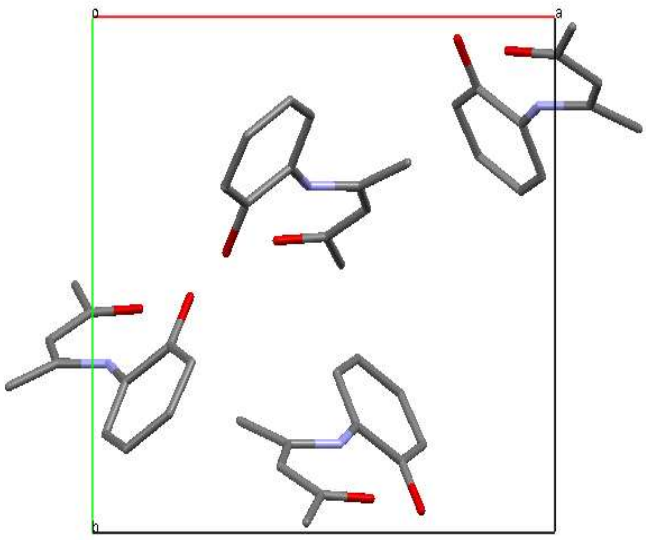

Figure 13. Packing diagram of the L_1 in the unit cell along the c-axis.

Table 2. Single crystal X-ray results for the L_1.

Chemical Formula	$C_{11}H_{12}NO_2$
CCDC No.	776073
Molecule Weight ($g.mol^{-1}$)	190,22
Crystal System	Orthorombic
Space Group	$P2_12_12_1$
a (Å)	11.225(6)
b (Å)	10.511(7)
c (Å)	8.849(3)
α/β/γ (o)	90/90/90
Volume V $(Å)^3$	1044,1(10)
Z	4
Density Dx ($Mg.m^{-3)}$	1,210
Absorption coefficient ı μ (mm^{-1})	0,084
R_{int}	0,0521
h, k, l range (°)	-13/13, -12/11, -7/10
θ_{min}-θ_{max}(°)	2,65 – 25,98
Reflections collected	4523
Independent reflections	1180
Parameters	132
R ; R (I >2σ (I))	0,0498 ; 0,1374
S	1,031
$\Delta\rho_{min.}$, $\Delta\rho_{max.}$($e/Å^3$)	-0,168 ; 0,359

Table 3. Selected bond lengths and angles of the L_1.

Bond Langets (Å)			
C1-O1	1.360(5)	C6-N1	1.411(5)
C1-C2	1.375(6)	C7-N1	1.351(4)
C1-C6	1.404(5)	C7-C9	1.355(5)
C2-C3	1.387(6)	C7-C8	1.508(5)
C3-C4	1.365(7)	C9-C10	1.409(5)
C4-C5	1.364(6)	C10-O2	1.259(4)
Bond Angles (°)			
O1-C1-C2	123.9(3)	C5-C6-C1	118.3(4)
O1-C1-C6	116.1(3)	C5-C6-N1	125.6(3)
C2-C1-C6	120.0(3)	C1-C6-N1	116.0(3)
C1-C2-C3	120.2(4)	N1-C7-C9	120.8(3)
C4-C3-C2	119.8(4)	N1-C7-C8	119.1(4)
C5-C4-C3	120.6(4)	C9-C7-C8	120.1(3)
C4-C5-C6	121.0(4)	C7-C9-C10	125.0(3)
O2-C10-C9	121.8(4)	C9-C10-C11	120.2(3)
O2-C10-C11	118.0(3)	C7-N1-C6	130.6(3)

3.5.2. Single Crystal X-Ray Studies of L_2 Ligand

The single crystal X-ray results of the L_2 are given in Table 4 and the selected bond lengths and bond angles of the ligand are given in Table 5

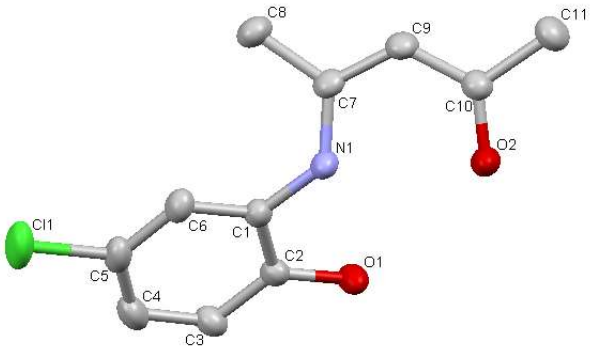

Figure 14. Crystal structure of the L_2.

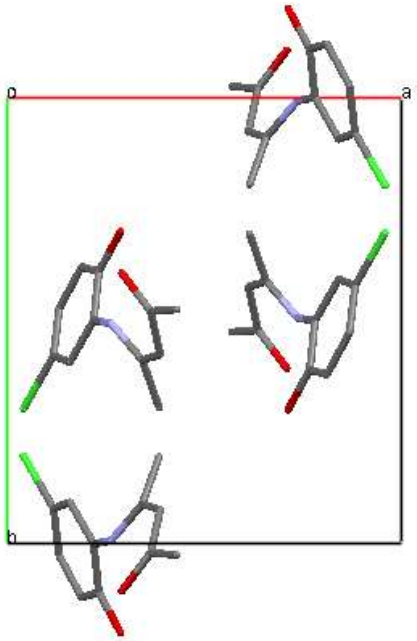

Figure 15. Packing diagram of the L_2 in the unit cell along the c-axis.

Table 4. Single crystal X-ray results for the L_2.

Chemical Formula	C_{11} H_{12} Cl N O_2
CCDC No.	776074
Molecule Weight (g.mol-1)	225.67
Crystal System	Monoklinik
Space Group	P 2_1/c
a (Å)	11.1020(5)
b (Å)	11.3117(6)
c (Å)	10.1827(5)
β(°)	115.750(3)
Volume V (Å)^3	1151.78(10)
Z	4
Density Dx (Mg.m$^{-3)}$	1.301
Elektron Sayısı (F_{000})	472
Absorption coefficient ı μ (mm^{-1})	0.311
R_{int}	0.0341
h, k, l range (°)	-13/13, -13/13, -12/12
θ_{min}-θ_{max}(°)	2,04 - 26.00
Reflections collected	16252
Independent reflections	2268
Parametres	150
R; R (I >2σ (I))	0.0376, 0.0991
S	1.021
$\Delta\rho_{min.}$, $\Delta\rho_{max.}$(e/Å^3)	-0.238; 0.049

Table 5. Selected bond lengths and angles of the L_2.

Bond Lenghts (Å)			
C1-C6	1.388(2)	C5-C6	1.374(2)
C1-C2	1.395(2)	C5-Cl1	1.7422(16)
C1-N1	1.412(2)	C7-N1	1.3375(19)
C2-O1	1.3508(18)	C7-C9	1.378(2)
C2-C3	1.386(2)	C7-C8	1.497(2)
C3-C4	1.373(2)	C9-C10	1.396(2)
C4-C5	1.374(3)	C10-O2	1.2580(19)
C10-C11	1.504(2)		
Bond Angels (°)			
C6-C1-C2	119.75(14)	C3-C4-C5	119.02(15)
C6-C1-N1	122.57(14)	C6-C5-C4	121.58(15)
C2-C1-N1	117.62(13)	C6-C5-Cl1	118.91(15)
O1-C2-C3	123.23(14)	C4-C5-Cl1	119.48(14)
O1-C2-C1	117.58(13)	C5-C6-C1	119.36(16)
C3-C2-C1	119.19(14)	N1-C7-C9	121.11(15)
C4-C3-C2	121.04(16)	N1-C7-C8	119.91(14)
C9-C7-C8	118.96(14)	O2-C10-C11	118.32(15)
C7-C9-C10	125.46(14)	C9-C10-C11	118.52(15)
O2-C10-C9	123.15(15)	C7-N1-C1	128.94(14)

4. Discussion

The IR spectra of L_1 and L_2 ligands, which have three teeth of ONO type, show similarities. The C=N peaks, which are characteristic peaks of Schiff bases, are 1606.1 cm^{-1} in L_1 ligand and 1607.5 cm^{-1} in L_2 ligand. When the XRD data of the ligands are analyzed, intramolecular hydrogen bonds are prominent. This situation prevents the OH peaks in the molecules from being seen clearly. While the vibrations belonging to the C-O bond are observed at 1240 cm^{-1} in the L_1 ligand, the vibrations belonging to the same bond are at 1243 cm^{-1} in the L_2 ligand. Similar results are also found in the literatures related to other ligands of the tridentate ONO type (Dhayalan et al., 2013).

Unlike the previously mentioned ligands, L_1 ligand does not contain hydrogen at the imine carbon. Therefore, the peaks between 8 and 9 ppm values found in the spectrum of other ligands are not observed in the spectrum of this ligand. Similar ligands in the literature that do not contain hydrogen at the imine carbon do not show peaks between these values (Zhang et al., 2022; Atabey et al., 2014). In this ligand, intramolecular hydrogen bonds play an important role in the shift values of OH protons. The phenolic proton peaks, which are normally observed at 4 to 8 ppm values, appeared at 12.2 ppm in this ligand. Likewise, the OH peaks attached to the aliphatic carbon are observed at 9.9 ppm instead of 3 to 6 ppm. The reason for these two shifts is intramolecular hydrogen bonding. The peaks belonging to the protons in the aromatic group of the ligand are observed between 6.7 and 7.2 ppm values.

The ^{1}H-NMR spectra of L_1 and L_2 ligands, whose structures are similar to each other, are similar in the main lines. In the L_2 ligand, the phenolic OH peak appears at 12.2 ppm, while the OH peak due to the aliphatic group is observed at 10.3 ppm. The reason why these peaks appear at lower than normal values is due to intramolecular hydrogen bonding. Unlike L_1 ligand, L_2 ligand shows a lack of a peak. The reason for this absence is the chlorine atom attached to the aromatic ring. The four peaks between 6.5 and 7.5 observed in the L_1 ligand are observed as three peaks in the L_2 ligand. This can be explained by the presence of chlorine atom in L_2 ligand where hydrogen atom is present in L_1 ligand (Yardan, 2010).

When the ^{13}C-NMR spectrum of the L_1 ligand is examined, it is seen that the peak belonging to the imine carbon appears in a lower area than the ligands previously examined. The main reason for this difference is the methyl group attached to the imine group. Since the electron

donating methyl group increases the screening on the carbon, the chemical shift value of this carbon is observed in the lower region compared to other ligands (Kargar et al., 2024; Yeşilbağ et al., 2024). The chemical shift values of the two nitrogen and oxygen bonded carbons of the aromatic ring in the structure are in the lower region compared to other aromatic carbons. The reason for this may be that nitrogen and oxygen have more electrons than hydrogen and the excitation energies of these electrons are lower.

As in the ^{1}H-NMR spectrum, L_1 and L_2 ligands, which have similar structures in the ^{13}C-NMR spectrum, can be compared. In the L_2 ligand, the peak belonging to the imine carbon is observed at 194 ppm. The fact that this value is in the lower range than other ligands with hydrogen at the imine carbon is due to the methyl group attached to the same carbon. Since the groups attached to the aromatic ring in the L_1 ligand increase the screening effect, the peaks of these carbons are observed in a higher area.

Two consecutive endothermic peaks are observed in the DTA curve of the crystalline L_1 ligand. The first of these peaks appeared at 196 °C and the second at 231 °C. It can be seen from the TG curve that the substance degrades in this temperature range. There is a mass loss of 98% in this range. Around 400 °C, it is observed that the degradation is completed.

In the DTA curve of L_2 ligand, two peaks are observed at 172 °C and 235 °C. It can be stated that the ligand decomposes in this temperature range. This is also consistent with the mass loss observed in the TG curve. Between 146 °C and 300 °C, 97% of the mass has decomposed. While a state change point was generally observed in the thermal analysis of the ligands, only one of the complexes showed a state change point. The other complexes decomposed without changing state. Mass loss up to 200 °C was observed in complexes with solvent molecules in the structure. L_1 and L_2 ligands degrade in one step.

Three absorptivity bands are observed in the electronic spectra of L_1 and L_2 ligands. It is an expected result that these two ligands, which have very similar structures, give maximum absorptivity at very close wavelengths.

The space group of the geometric shape of the L_1 is $P2_12_12_1$. There are 4 molecu,s in the unit cell of the crystal system of the L_1 ligand. The unit cell angles are equal to each other and 90 degrees. The unit cell lengths are a = 11.225, b = 10.511, c = 8.849 Å. These values indicate that the unit cell is in the orthorhombic crystal system. The first striking feature of the L_1 ligand is that the structure is not planar. The aromatic ring and the aliphatic parts of the ligand, which has three ONO-type teeth, are in different planes. An important part of the bending of the structure takes place over the nitrogen atom. Here the angle between C6-N1-C7 atoms is 130.6°. The space group of the geometric shape of the L_2 is $P2_1/c$. There are four molecules in the unit cell of the crystal system of the ligand. The unit cell lengths of the crystal are a = 11.1020, b = 11.3117, c = 10.1827 Å. The L_2 ligand is not planar like the L_1 ligand which has a similar structure. The molecule is bent over the nitrogen atom connecting the aromatic ring and the aliphatic group. Here the angle between C7-N1-C1 atoms is 128.94°.

5. Conclusions

IR, UV-Vis, ^{1}H-NMR, ^{13}C-NMR, thermal analysis and single crystal X-ray diffraction data of the ligands used during the study were compared and their structures were elucidated. Comparison of these molecules can give important datas for spectroscopic and thermal studies. Indeed, these two molecules, which look very similar at first glance, have quite different values when we look at their three-dimensional structures. And other small differencies from the studies support the similarity of two molecules.

Conflicts of Interests
Authors declare that there is no conflict of interests

Financial Disclosure
Author declare no financial support.

Statement contribution of the authors
This study's experimentation, analysis and writing, etc. all steps were made by the authors.

Acknowledgement
We would like to thank Balikesir University, Faculty of Art and Science, Department of Chemistry and Department of Physics and Altınoluk Vocational School for their support in the conduct of this research.

References

1. Abdel-Rahman, L. H., Abu-Dief, A. M., Basha, M., & Abdel-Mawgoud, A. A. H. (2017). Three novel Ni(II), VO(II) and Cr(III) mononuclear complexes encompassing potentially tridentate imine ligand: synthesis, structural characterization, DNA interaction, antimicrobial evaluation and anticancer activity. Applied Organometallic Chemistry, 31 (11), e3750. https://doi.org/10.1002/aoc.3750
2. Atabey, H., Findik, E., Sari, H., & Ceylan, M. (2014). Comparison of chelating ability of NO-, NS-, ONS-, and ONO-type schiff base derivatives and their stability constants of bis-complexes with copper(II). Turkish Journal of Chemistry, 38 (1), 109–120. https://doi.org/10.3906/kim-1303-65
3. Azadi, S., Azizipour, E., Amani, A. M., Vaez, A., Zareshahrabadi, Z., Abbaspour, A., Firuzyar, T., Dortaj, H., Kamyab, H., Chelliapan, S., & Mosleh-Shirazi, S. (2024). Antifungal activity of Fe3O4@SiO2/Schiff-base/Cu(II) magnetic nanoparticles against pathogenic Candida species. Scientific Reports, 14 (1), 5855. https://doi.org/10.1038/s41598-024-56512-5
4. Choudhary, M. (2023). Synthesis and characterization of phenoxy-bridged copper(II) complexes: Structural features, magnetic, thermal and redox properties, and theoretical studies. Inorganica Chimica Acta, 557, 121708. https://doi.org/10.1016/j.ica.2023.121708
5. Dalei, G., Pattanaik, C., Patra, R., Jena, D., Das, B. R., & Das, S. (2024). Chitosan xerogel embedded with green synthesized cerium oxide nanoparticle: An effective controlled release fertilizer for improved cabbage growth. International Journal of Biological Macromolecules, 282, 136704. https://doi.org/10.1016/j.ijbiomac.2024.136704
6. Dhayalan, V., Murakami, R., & Hayashi, M. (2013). Practical preparation of chiral keto-imine type ONO Schiff base ligands. Tetrahedron-Asymmetry, 24 (9–10), 543–547. https://doi.org/10.1016/j.tetasy.2013.03.017
7. Kargar, H., Fallah-Mehrjardi, M., & Munawar, K. S. (2024). Metal complexes incorporating tridentate ONO pyridyl hydrazone schiff base ligands: crystal structure, characterization and applications. Coordination Chemistry Reviews, 501, 215587. https://doi.org/10.1016/j.ccr.2023.215587
8. Li, Y.-D., Kuang, J.-H., Qin, H.-B., Liu, K.-X., Fan, X., Li, Z.-Y., & Yuan, L. (2022). A novel salicylaldehyde schiff-base fluorescent probe for selective detection of Cu²⁺ Ion. Chinese Journal Of Structural Chemistry, 41 (3), 2203132–2203136. https://doi.org/10.14102/j.cnki.0254-5861.2011-3288
9. Moreira, J. M., Rodrigues, R., Trindade, M. A. G., dos Santos, K. C., da Silva, M. M., Tirloni, B., Brandl, C. A., Paveglio, G. C., Roman, D., & de Carvalho, C. T. (2025). Characterization (XRD/TGA-DSC) and assessment of calf thymus DNA interaction with single-crystalline novel complexes from Schiff base ligands. Inorganica Chimica Acta, 575, 122443. https://doi.org/10.1016/j.ica.2024.122443
10. Nassar, A. A., El-Sawaf, A. K., & El-Samanody, E.-S. A. (2024). A new Ni^{2+}, Pd^{2+}, and Pt^{2+} coordination compounds of carbothiohydrazide based chelating agent: Synthesis, characterization, crystal structure, DFT-TDFT calculations, antioxidant, and antimircrobial activities. Inorganic Chemistry Communications, 170, 113405. https://doi.org/10.1016/j.inoche.2024.113405
11. Puthilibai, G., Devatarika, V., Haewon, B., Behura, S. S., Lautre, H. K., Subha, V., Sangwan, P., & Sunil, J. (2023). Synthesized and hypothesized schiff base ligand and its metal(ii) complexes dna binding mode. Bulletin of the Chemical Society of Ethiopia, 37 (5), 1133–1139. https://doi.org/10.4314/bcse.v37i5.6
12. Sharma, S., Sharma, P., Singh, V., Vaishali, Vashistha, V. K., Das, D. K., Pal, K., Kumar, N., & Devi, P. (2024). Exploitation of pyrazole C-3/5 carbaldehydes towards the development of therapeutically valuable scaffolds: A review. Chemical Papers, 78 (11), 6287–6314. https://doi.org/10.1007/s11696-024-03534-y
13. Somashekar, M. N., Chetana, P. R., Chethan, B. S., Rajegowda, H. R., Cooper, M. A., Ziora, Z. M., Lokanath, N. K., Ganapathy, P. S. S., & Srinatha, B. S. (2022). Synthesis and characterization of Zinc(II) complex with ONO donor type new phenylpropanehydrazide based ligand: Crystal structure, Hirshfeld surface analysis, DFT, energy frameworks and molecular docking. Journal of Molecular Structure, 1255, 132429. https://doi.org/10.1016/j.molstruc.2022.132429
14. Tian, Z., Cui, S., Liu, G., Wang, R., & Pu, S. (2016). A new fluorescent sensor for Zn2+ based on diarylethene with a 4-diethylamino-salicylaldehyde Schiff base unit. Journal of Physical Organic Chemistry, 29 (8), 421–429. https://doi.org/10.1002/poc.3552
15. Wang, Q., Jiang, C., Wang, H., Jin, X., Tao, Y., Lu, J., Du, J., & Wang, H. (2024). A multifunctional soybean protein isolates crosslinked gelatins composite mulch film: Fabrication, characterization, and application. International Journal of Biological Macromolecules, 282, 137252. https://doi.org/10.1016/j.ijbiomac.2024.137252

16. Wang, Y.-R., Yang, L., Wang, D.-T., Li, A.-P., Zhang, S.-Y., Qin, L.-L., Bian, Q., Zhang, Z.-J., Ding, Y.-Y., Zhou, H., Peng, D., Wang, G.-H., & Liu, Y.-Q. (2024). Design and synthesis aldehydes-thiourea and thiazolyl hydrazine derivatives as promising antifungal agents against *Monilinia fructicola*. Pest Management Science. 81, 174-184. https://doi.org/10.1002/ps.8417
17. Yardan, A. (2010). Çok dişli schiff bazlarının sentezi ve bazı geçiş metalleri (M= Ni^{2+}, Zn^{2+}, Cd^{2+} ve Cu^{2+}) ile yaptığı koordinasyon bileşiklerinin hazırlanması, yapılarının aydınlatılması ve termal davranışlarının incelenmesi. PhD. thesis, Balikesir University, Turkey.
18. Yardan, A., Hopa, C., Yahsi, Y., Karahan, A., Kara, H., & Kurtaran, R. (2015). Two new heterodinuclear schiff base complexes: synthesis, crystal structure and thermal studies. Spectrochimica Acta Part A-Molecular and Biomolecular Spectroscopy, 137, 351–356. https://doi.org/10.1016/j.saa.2014.08.091
19. Yardan, A., Yahsi, Y., Kara, H., Karahan, A., Durmus, S., & Kurtaran, R. (2014). Synthesis, characterization, crystal structure, magnetic studies of a novel polymeric zig-zag chain copper (II) complex. Inorganica Chimica Acta, 413, 55–59. https://doi.org/10.1016/j.ica.2014.01.006
20. Yeşilbağ, S., Kansız, S., Dege, N., & Ağar, E. (2024). Structural investigation and hirshfeld surface analysis of two [ONO]-type schiff bases. Journal of Structural Chemistry, 65 (3), 464–477. https://doi.org/10.1134/S0022476624030041
21. Zhang, G., Zhang, Y., Zhang, H., & Wen, Y. (2022). Performance comparison of [ONS]-type and [ONO]-type schiff bases in the acylphosphonylation of aldehyde. Chemistryselect, *7* (9), e202104394. https://doi.org/10.1002/slct.202104394
22. Zhang, X., Gao, M., Dong, Y., Pan, L., Zhai, M., & Jin, L. (2024). Novel aminocoumarin-based schiff bases: high antifungal activity in agriculture. Chemistry & Biodiversity, 21, e202401390. https://doi.org/10.1002/cbdv.202401390